Two-dimensional lattice of blue-detuned atom traps using a projected Gaussian beam array

M. J. Piotrowicz, M. Lichtman, K. Maller, G. Li,[*] S. Zhang,[†] L. Isenhower, and M. Saffman[‡]
Department of Physics, University of Wisconsin, 1150 University Avenue, Madison, Wisconsin 53706, USA
(Received 27 May 2013; published 24 July 2013)

We describe a blue-detuned optical lattice for atom trapping which is intrinsically two-dimensional, while providing three-dimensional atom localization. The lattice is insensitive to optical phase fluctuations since it does not depend on field interference between distinct optical beams. The array is created using an arrangement of weakly overlapping Gaussian beams that creates a two-dimensional array of dark traps which are suitable for magic trapping of ground and Rydberg states. We analyze the spatial localization that can be achieved and demonstrate trapping and detection of single Cs atoms in 6- and 49-site two-dimensional arrays.

DOI: 10.1103/PhysRevA.88.013420 PACS number(s): 37.10.Gh, 37.10.Jk, 03.67.−a

I. INTRODUCTION

Arrays of neutral atom qubits in optical traps are being actively developed for implementing multiqubit quantum information processing (QIP) devices [1–4]. Far-detuned optical traps provide strong confinement with low photon scattering rates and low decoherence [5]. Red-detuned traps localize atoms at a maximum of the optical intensity, which leads to higher photon scattering rates and light shifts on atomic levels which are used for qubit encoding and control. Blue-detuned traps confine atoms at a local minimum of the optical intensity. This reduces photon scattering and light shifts and is of particular interest for experiments using Rydberg atom excitation since blue-detuned configurations allow for simultaneous trapping of both ground and Rydberg excited states [6]. This capability will be important for future scalable QIP devices based on Rydberg-state-mediated quantum gates [7–9] as well as adiabatic approaches based on Rydberg dressing [10] or dissipative interactions [11] which require long-term occupancy of Rydberg states.

Projected arrays of dipole traps have been demonstrated using either microlenses [12], holographic methods [13], or diffractive optics [14,15]. Several experiments in recent years have demonstrated loading of single atoms into small arrays of optical traps [13,14] and into larger optical lattices using either stochastic loading [16] or Bose-Einstein condensate to Mott insulator techniques [17–19]. For QIP applications we would like the trap array to have the following characteristics. It should be scalable to a large number of trapping sites, two-dimensional to minimize crosstalk from neighboring planes of trapped atoms, and stable against trap position drifts due to optical phase fluctuations, and, particularly for experiments with Rydberg atoms [2], we wish to use blue-detuned traps.

Most optical lattices use interference of beams that are counter-propagating, or co-propagating at a small angle, to create the trap array [20]. With this approach the positions of the trap sites are directly sensitive to optical path-length drifts in the apparatus, causing differential phase shifts between beams. Although active stabilization is possible [21], this has not been demonstrated in single-atom experiments. Alternatively, one of the sites can be used to monitor lattice drifts [19]. A diffractive method was demonstrated in [17], which suppresses phase sensitivity of the lattice sites. That method provides a two-dimensional trap array with localization out of the plane being provided by a separate orthogonally propagating beam.

Here we propose and demonstrate an approach that is scalable to many sites, creates an intrinsically two-dimensional array of traps which localize the atoms in all three dimensions, and is blue-detuned for use with Rydberg atoms. This work builds on recent experience with atom trapping in blue-detuned bottle beam traps (BBTs) [22–25]. A possible approach would be to create multiple copies of a BBT using a diffractive beam splitter (DBS). Such an array confines atoms with two trap walls between each trapped atom. This leads to a lower density of sites than we would like. Instead we use a DBS to create a weakly overlapping Gaussian beam array (GBA). The atoms are localized in the intensity minima between beams while the overlap regions create saddle potentials which laterally trap the atoms, as shown in Fig. 1. Localization out of the plane is provided by diffractive spreading of the beams.

The rest of this paper is organized as follows. In Sec. II we describe the design of the GBA and present two versions, which we refer to as half- and full-incoherent. We also compare the performance in terms of trap depth and localization with that of a conventional optical lattice. In Sec. III we describe the optical system used to create the array and in Sec. IV we show that single atoms can be effectively trapped. We conclude with an outlook in Sec. V.

II. GAUSSIAN BEAM ARRAY DESIGN

In this section we present the design and analysis of an array of blue-detuned traps based on a weakly overlapping GBA. The geometry is shown in Fig. 1. Each beam has a waist parameter w_0 (radius where the intensity is $1/e^2$ of the maximum) and the array periodicity is d. We frequently use the ratio $s = d/w_0$ to characterize the array. We use the term weakly overlapping to describe the situation where $d > w_0$ and the ratio is $s \sim 2$. For this value of s the overlap between neighboring beams is significant, and indeed defines the trap sites, while the overlap between beams separated by larger distances is negligible.

[*]Present address: Institute of Opto-Electronics, Shanxi University, 92 Wucheng Road, Taiyuan 030006, Shanxi Province, China.
[†]Present address: KLA Tencor, One Technology Drive, Milpitas, California 95035, USA.
[‡]msaffman@wisc.edu

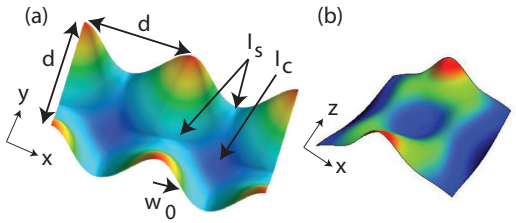

FIG. 1. (Color online) Intensity distribution of Gaussian beam array in the x-y (a) and x-z (b) planes. Beams propagate along the z axis, giving an array of traps lying in the x-y plane. The trap array has periodicity d and forms atom traps at the center of each four-beam plaquette where the intensity is I_c. Lateral confinement in the x-y plane is provided by the saddles with intensity I_s. Localization normal to the x-y plane along z is provided by diffractive spreading of the beams.

In order to suppress coherent interference between neighboring beams we analyze two types of arrays. In the first, which we call half-incoherent, neighboring beams have orthogonal polarizations so we can add their intensities when calculating the trap depth. This statement is based on the assumption that the beams are far detuned from the nearest atomic resonance so that vector and tensor contributions to the ground-state polarizability are negligible. The remaining field interference terms are between beams on the diagonal of a unit cell. Their separation is $\sqrt{2}d$, whereas neighboring beams are separated by only d, so the interference term along the diagonal is strongly suppressed compared to neighboring beams separated by d. Nevertheless, the sensitivity to phase variations between beams can lead to variations in the trap intensity at the center of each unit cell.

The second type of array, which we call full-incoherent, effectively removes the residual phase sensitivity of the half-incoherent array. In this case we use a combination of orthogonal polarizations and different laser frequencies so that there is no field interference between neighbors or between diagonal neighbors. As long as the frequency difference is large compared to the trap vibrational frequencies, we can treat the array potential as being due to the incoherent sum of the beams. The remaining field interference effects are due to beams separated by $2d$ or more, and for our parameters these terms are negligible.

For both the half-incoherent and the full-incoherent arrays the use of different polarizations and frequencies also serves an additional purpose. If the entire array were due to a uniformly polarized coherent field, the Talbot effect would lead to multiple copies of the array along the normal z axis. This would allow for trapping in multiple planes and we would not have a two-dimensional array of traps. The half- and full-incoherent designs effectively suppress the Talbot effect and we get a single plane of traps.

A. Half-incoherent array

Consider a unit cell as shown in Fig. 1 with neighboring beams having orthogonal polarization states. At the saddle point along each side of the unit cell the intensity is approximately

$$I_s = 2I_0 e^{-2(d/2)^2/w_0^2} = 2I_0 e^{-d^2/2w_0^2}, \tag{1}$$

where I_0 is the peak intensity of one beam. If diagonally opposite beams are in phase (this is the worst case, giving the lowest trapping potential), the intensity at the center of the unit cell where an atom is trapped is approximately

$$I_c = 2I_0\left(2e^{-(d/\sqrt{2})^2/w_0^2}\right)^2 = 8I_0 e^{-d^2/w_0^2}. \tag{2}$$

In Eqs. (1) and (2) we neglect contributions from farther-away beams in neighboring unit cells; for the saddle intensity we only account for the two nearest beams, and for the center intensity we account for all four beams in one unit cell.

The trap depth is proportional to the difference between these two intensities, which is

$$I_t = I_s - I_c = I_0 2e^{-s^2/2}\left(1 - 4e^{-s^2/2}\right). \tag{3}$$

Figure 2(a) shows the trap depth as a function of s. The trap depth has a maximum at $s_0 = (2\ln 8)^{1/2} \simeq 2.04$. Using $s = s_0$ we find $I_s = I_0/4$, $I_c = I_0/8$, and $I_t = I_0/8$.

We are most interested in the trap depth as a function of w_0 for a fixed optical power and fixed lattice period d. Defining the average intensity in a unit cell of area d^2 as

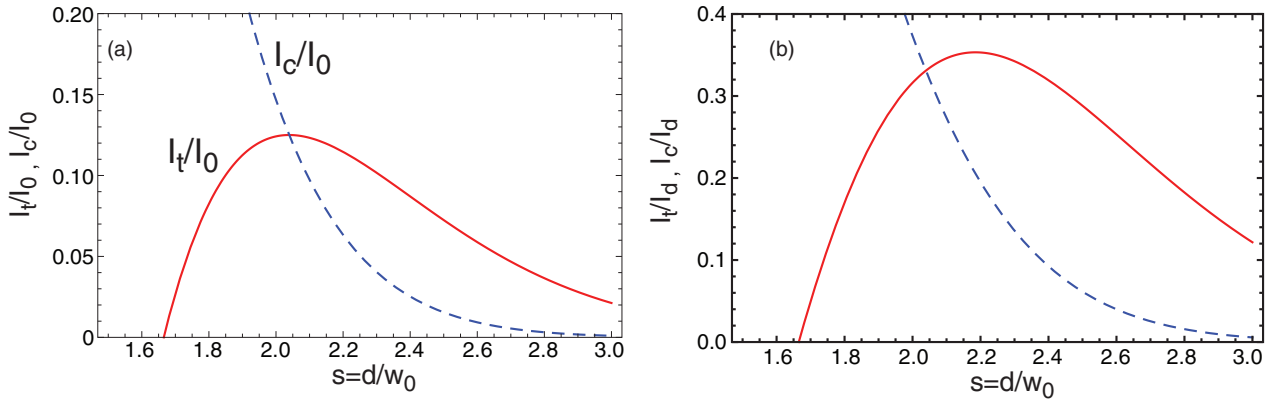

FIG. 2. (Color online) Normalized trapping depth [solid (red) curve] and intensity at trap center [dashed (blue) curve] versus normalized array period for half-incoherent array. Variation at constant peak intensity I_0 (a) and at constant average intensity I_d (b).

$I_d = \frac{P}{d^2} = \frac{\pi w_0^2 I_0}{2d^2} = \frac{\pi I_0}{2s^2}$, the trap intensity is

$$I_t = I_d \times \frac{4s^2 e^{-s^2/2}}{\pi}\left(1 - 4e^{-s^2/2}\right). \tag{4}$$

Figure 2(b) shows the trap depth, which reaches a maximum of $I_t/I_d = 0.35$ at $s = 2.19$. Note that the calculated trap depth in Fig. 2 is based on a worst-case assumption. If the diagonal beams were out of phase, we would get $I_c = 0$ and the peak trap depth would be about twice as large. It can also be verified that contributions from farther-away beams have a negligible impact on the plots in Fig. 2.

In addition to the trap depth, it is important to know the spatial localization and oscillation frequencies. Using the approximation of the potentials at the trap center given in [6] we get the effective spring constants

$$\kappa_x = \frac{32|U_d|}{\pi d^2} s^4 (s^2 - 2) e^{-s^2}, \tag{5a}$$

$$\kappa_y = \kappa_x, \tag{5b}$$

$$\kappa_z = \frac{32\lambda^2 |U_d|}{\pi^3 d^4} s^6 (s^2 - 1) e^{-s^2}, \tag{5c}$$

with $U_d = \frac{\alpha}{2\epsilon_0 c} I_d$; α is the atomic polarizability in SI units, and λ is the wavelength of the trapping light. The x axis is directed from the trap center towards a neighboring side. The corresponding oscillation frequencies are $\omega = \sqrt{\kappa/m_a}$, with m_a the atomic mass.

The time-averaged position variances are found from $\frac{1}{2}\kappa_j \sigma_j^2 = \frac{1}{2}\kappa_j \langle r_j^2 \rangle = \frac{1}{2} k_B T$, with T the atomic temperature. They are

$$\sigma_x^2 = \frac{\pi k_B T}{32|U_d|} \frac{e^{s^2}}{s^2(s^2-2)} w_0^2 = \sigma_{x0}^2 \frac{e^{s^2}}{s^4(s^2-2)}, \tag{6a}$$

$$\sigma_y^2 = \sigma_x^2, \tag{6b}$$

$$\sigma_z^2 = \frac{\pi k_B T}{32|U_d|} \frac{e^{s^2}}{s^2(s^2-1)} L_R^2 = \sigma_{z0}^2 \frac{e^{s^2}}{s^6(s^2-1)}, \tag{6c}$$

with $\sigma_{x0} = (\frac{\pi d^2 k_B T}{32|U_d|})^{1/2}$ and $\sigma_{z0} = (\frac{\pi^3 d^4 k_B T}{32\lambda^2 |U_d|})^{1/2}$. The optimal confinement values are $\sigma_x = 1.31\,\sigma_{x0}$ at $s = 2$ and $\sigma_z = 0.53\,\sigma_{z0}$ at $s = (\frac{5+\sqrt{13}}{2})^{1/2} \simeq 2.07$. Figure 3 shows the dependence of confinement on the parameter s.

B. Full-incoherent array

If we use two laser frequencies, we can arrange for all neighboring beams, both along an edge and across a diagonal of a unit cell, to combine incoherently. An optical layout which implements this is shown in Sec. III. For this arrangement the saddle and center intensities are

$$I_s = 2I_0 e^{-s^2/2} \tag{7}$$

and

$$I_c = 4I_0 e^{-2(d/\sqrt{2})^2/w_0^2} = 4I_0 e^{-s^2}. \tag{8}$$

Compared with (1) and (2) we see that the saddle intensity is unchanged, but the intensity at the center is reduced by a factor of 2. Reduction of the center intensity increases the trap depth and, also, eliminates the phase dependence, which would lead to unwanted structure near the center of the trap.

The trap depth is

$$I_t = I_0 \times 2e^{-s^2/2}\left(1 - 2e^{-s^2/2}\right) = I_d \times \frac{4s^2 e^{-s^2/2}}{\pi}\left(1 - 2e^{-s^2/2}\right). \tag{9}$$

Figure 4 shows the trap depth as a function of s. The maximum of $I_t/I_d = 0.51$ occurs at $s = 1.92$. For the same average intensity the full-incoherent array has an approximately 30% larger trap depth than the half-incoherent array.

Following the same steps as for the half-incoherent array, we find for the spring constants and spatial localization

$$\kappa_x = \frac{32|U_d|}{\pi d^2} s^4 (s^2 - 1) e^{-s^2}, \tag{10a}$$

$$\kappa_y = \kappa_x, \tag{10b}$$

$$\kappa_z = \frac{16\lambda^2 |U_d|}{\pi^3 d^4} s^8 e^{-s^2} \tag{10c}$$

and

$$\sigma_x^2 = \sigma_{x0}^2 \frac{e^{s^2}}{s^4(s^2-1)}, \tag{11a}$$

$$\sigma_y^2 = \sigma_x^2, \tag{11b}$$

$$\sigma_z^2 = \sigma_{z0}^2 \frac{2e^{s^2}}{s^8}. \tag{11c}$$

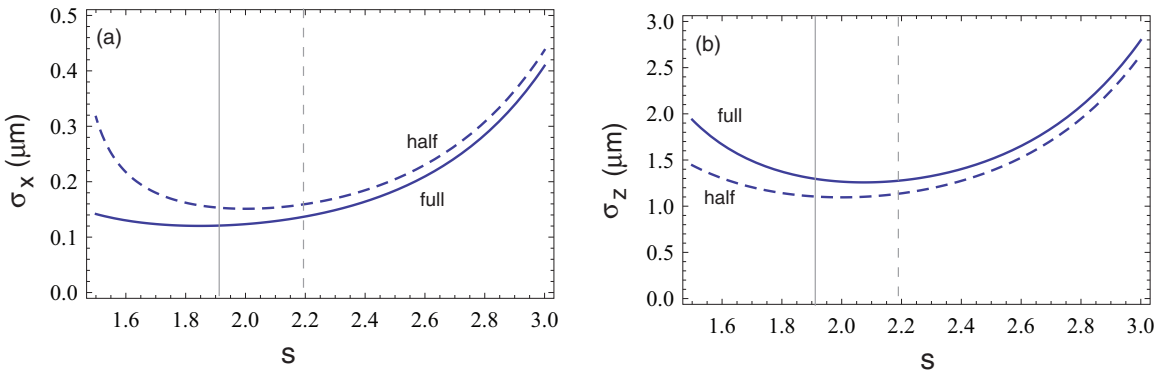

FIG. 3. (Color online) Standard deviation of x position (a) and z position (b) for a half-incoherent array (dashed curves) and full-incoherent array (solid curves). Vertical lines are at the s values for which the trap depths are maximized. Parameters are $\lambda = 0.78\ \mu$m, $d = 3.6\ \mu$m, $T = 10\ \mu$K, and $U_t = k_B \times 300\ \mu$K.

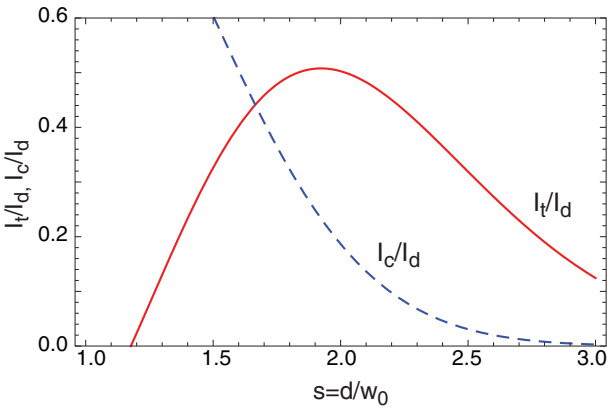

FIG. 4. (Color online) Normalized trapping depth (solid curve) and intensity at trap center (dashed curve) versus normalized array period for full-incoherent array. The plot assumes constant average intensity I_d.

The optimal confinement values are $\sigma_x = 1.04\,\sigma_{x0}$ at $s = \sqrt{2+\sqrt{2}} \simeq 1.85$ and $\sigma_z = 0.65\,\sigma_{z0}$ at $s = 2$.

Comparing the half- and full-incoherent arrays we see that the full-incoherent case has a better trap depth and transverse localization for the same optical power. The axial localization is worse for the full-incoherent array, but this is a less important figure of merit than the transverse localization when addressing beams that propagate along z. We conclude that the full-incoherent array should give a somewhat better performance for qubit control and, also, is less sensitive to parasitic light scattering and optical imperfections.

C. Comparison with optical lattice

The spatial average of the intensity in a unit cell I_d is related to the effective trapping intensity I_t by

$$I_t^{\rm hi} = I_d \times \frac{4s^2 e^{-s^2/2}}{\pi}\left(1 - 4e^{-s^2/2}\right), \tag{12}$$

$$I_t^{\rm fi} = I_d \times \frac{4s^2 e^{-s^2/2}}{\pi}\left(1 - 2e^{-s^2/2}\right), \tag{13}$$

where hi and fi stand for half- and full-incoherent, respectively. The maximum optical efficiency is $(I_t/I_d)_{\rm hi} = 0.35$ and $(I_t/I_d)_{\rm fi} = 0.51$. These ratios can be compared with a traditional optical lattice formed by interfering plane waves. The comparison depends on the dimensionality and type of optical lattice. For the simplest case of a one-dimensional lattice the effective trapping intensity is the difference between the maximum and the minimum intensities, which is twice the average intensity for a sinusoidal lattice. Thus the full-incoherent GBA implementation has a relative efficiency of at best $0.51/2 = 25.5\%$.

The GBA appears to be more favorable when we consider the performance in three dimensions. We consider two types of coherent lattice. A standard counterpropagating geometry uses three beams, each retroreflected to create a $d = \lambda/2$ lattice period in all three dimensions. The power required is 3 times P_1, the power of each beam, so the intensity averaged over a unit cell is $I_d = 3P_1/(\lambda/2)^2 = 12P_1/\lambda^2$. The trap depth is $I_t = 4I_1$ so $I_t/I_d = \lambda^2 I_1/3P_1$, and putting $I_1 = P_1/(\lambda/2)^2$ we get $I_t/I_d = 4/3$. The GBA has a relative efficiency of $0.51/(4/3) = 39\%$. It is also possible to create longer period lattices by interfering pairs of beams at an acute angle $\theta < \pi$ as in [16]. In this case $I_t = 4I_1 = 4P_1/d^2$, $I_d = 6P_1/d^2$, and $I_t/I_d = 2/3$. The GBA has a relative efficiency of $0.51/(2/3) = 78\%$.

We see that the GBA has a lower efficiency than a standard optical lattice. The benefit is the absence of phase sensitivity as regards the position of the trap sites as well as the ability to project the lattice onto the atomic sample using optical access from a single side.

III. OPTICAL IMPLEMENTATION

A straightforward approach to creating an array of Gaussian beams is to start with a single laser beam and use a Dammann grating [26] to replicate the beam. Gratings that can create several hundred equal-intensity beams are readily available commercially. Unfortunately, a single Dammann grating does not work well for creating an array of overlapping beams. The diffractive spreading angle of a Gaussian beam of waist w_0 is $\theta_d = \lambda/\pi w_0$. The angular separation of the beams from a grating of period Λ is $\theta_g = \lambda/\Lambda$. In order to achieve $s = d/w_0 \simeq 2$, which we identified in the previous section as the optimal spacing, we need $\theta_g/\theta_d \simeq 2$. However, this implies that $\theta_g/\theta_d = \pi w_0/\Lambda \simeq 2$ or $\Lambda \simeq \frac{\pi}{2} w_0$. In other words, the grating period is comparable to the waist of the Gaussian beam illuminating the grating. In this regime standard Dammann gratings do not perform well and lead to large distortions of the diffracted spot array. Our tests show that the beam quality after the grating is good when $s \gtrsim 4$.

While it should be possible to design a custom grating that works well for this application, we have instead used a Dammann grating with $\Lambda \simeq \pi w_0$, giving $s = 4$, followed by beam displacement optics as shown in Fig. 5, to reduce the beam spacing to $s = 2$. The calcite beam displacement elements serve the additional function of giving neighboring beams orthogonal polarizations for the array designs described above.

We have implemented a half-incoherent GBA as shown in Fig. 6. A single $\rm TEM_{00}$ Gaussian beam is divided on a

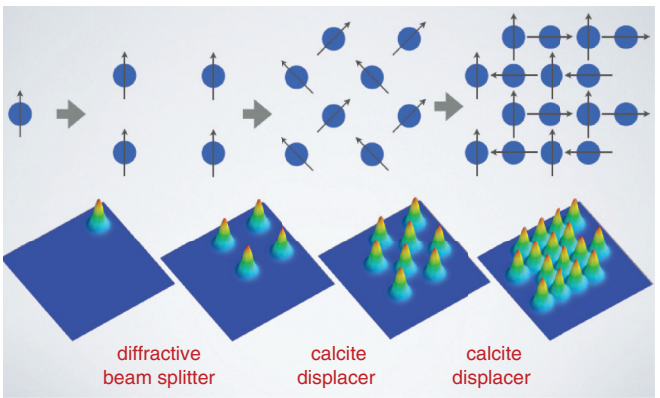

FIG. 5. (Color online) Making a half-incoherent array with a Dammann grating and calcite displacers. The illustration shows creation of a 16-beam array with six trapping sites. Arrows indicate the direction of linear polarization of each beam.

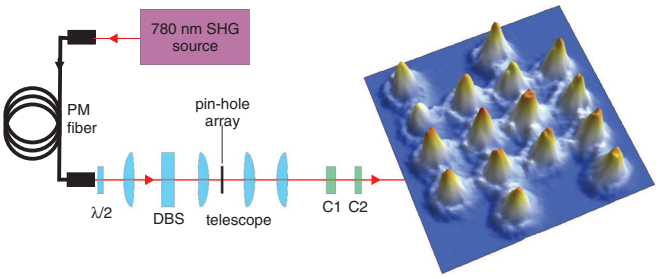

FIG. 6. (Color online) Optical system for creating a half-incoherent GBA with six trapping sites. The intensity image shows the array before focusing onto the atoms with parameters $\lambda = 0.78\ \mu$m, $d = 250\ \mu$m, $w_0 = 120\ \mu$m, and $s = 2.1$. The 780-nm source is based on a frequency-doubled, single-frequency, 1560-nm laser.

Dammann grating, which we refer to as a DBS (Holo/Or MS-248-X-Y-A). The grating is placed in the front focal plane of a lens to create an array of four parallel beams with separation $d = 500\ \mu$m and $s \simeq 4.2$. The pin-hole array suppresses all non-first-order beams from the DBS. This is then followed by two pieces of calcite. The first, thicker piece, C1, is cut to give a lateral displacement of $500/\sqrt{2} = 354\ \mu$m. This is followed by a second, thinner calcite, C2, rotated by 45° relative to C1, which gives a displacement of $500/2 = 250\ \mu$m. The net result is an array with $d = 250\ \mu$m and $s \simeq 2.1$, with neighboring beams having orthogonal linear polarizations. An implementation of this design to create 16 beams and six trap sites is shown in Fig. 6. The 16-beam array is then imaged onto a cloud of cold Cs atoms in a Pyrex cell with a multielement NA = 0.4 lens that is designed to compensate for cell wall aberrations to give diffraction limited focusing. The lattice spacing at the atoms is $d = 3.8\ \mu$m.

We have also implemented the full-incoherent array design, where the nearest-neighbor beams come from two different laser sources (or are shifted in frequency by acousto-optic modulators) and the next-nearest neighbors have different polarizations. The scheme of the optical realization is presented in Fig. 7. Two separated arms create 4×4 Gaussian arrays that are combined using a polarizing beam splitter (PBS). Finally, this array is shifted by a single calcite to create a 64-beam array with 49 trapping sites. The other parameters for the trap array are similar to those for the half-incoherent case described above.

IV. ATOM TRAPPING DEMONSTRATION

We have demonstrated that both the half- and the full-incoherent arrays described above are suitable for trapping of cold Cs atoms. We use a double magneto-optical trap (MOT) apparatus with a two-dimensional MOT feeding a three-dimensional MOT in a differentially pumped Pyrex vacuum cell. We load the GBA from the three-dimensional MOT, which is based on a standard six-beam configuration. The MOT is cooled to 10–20 μK with 10 ms of polarization gradient cooling (PGC), giving number densities of $\sim 2 \times 10^9$ cm^{-3}. The 780-nm trapping light is switched on at the beginning of the PGC phase when the atomic density is highest, and at the end of the loading phase all MOT and PGC light is switched off to allow the atoms that are not trapped to fall

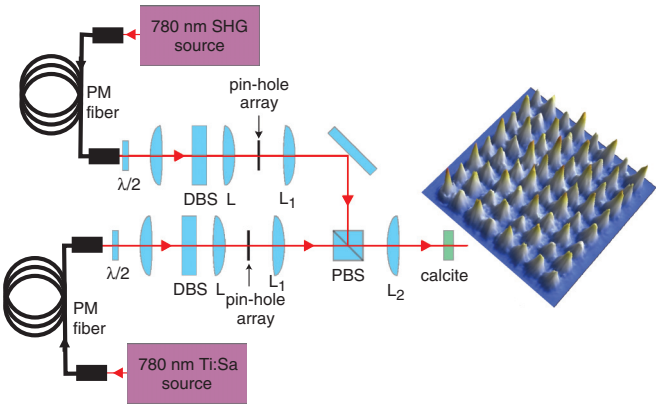

FIG. 7. (Color online) Experimental setup for creating a full-incoherent GBA with 49 trapping sites. Two 4×4 arrays created by diffractive elements (DBS) are combined by a polarizing beam-splitter (PBS). Lenses L_1 and L_2 create a 1:1 telescope to image the arrays onto the calcite that combined them into a 64-beam array. Pin-hole arrays are placed in the foci of lenses (L) to block unwanted zeroth and higher orders of diffraction from the DBS. The spatial parameters of the resulting array are the same as in Fig. 6.

away. The MOT and GBA loading takes about 0.7 s. Trapped atoms are detected by turning on the PGC light and imaging the scattered fluorescence onto an electron multiplying charge-coupled device (EMCCD) camera. The 852-nm fluorescence is collected through the same lens used to project the GBA onto the atoms and separated with a dichroic filter from the 780-nm trapping light. Typical detection parameters are detuning of -39 MHz $= -7.5\gamma$ from the $6s_{1/2},\ f = 4 \leftrightarrow 6p_{3/2},\ f = 5$ transition with $I \simeq 2.7 I_{\rm sat}$, where $I_{\rm sat}$ is the saturation intensity, and scattered light is collected for 50 ms. EMCCD exposure times as short as 5 ms are sufficient to resolve single-atom signals.

A. Half-incoherent array

We first describe results using the six-site half-incoherent array. The trap depth is calculated from Eq. (3). For Cs atoms at a trap-light wavelength of 780 nm the scalar polarizability is $\alpha_0^{\rm cgs} = -240 \times 10^{-24}$ cm^3. We transmit 3 W of 780-nm light through a single-mode polarization maintaining fiber. The

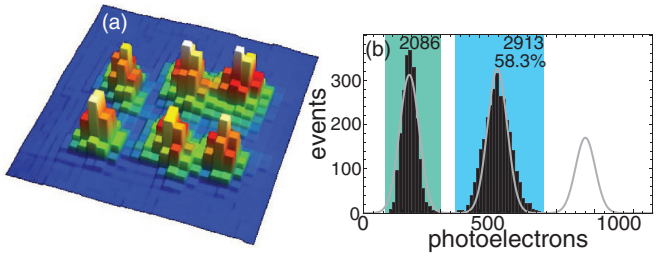

FIG. 8. (Color online) Fluorescence image (a) and atom number histogram (b) in the six-site half-incoherent array. The image is an average of 105 of 5000 events where all six sites loaded a single atom. Each pixel is $0.63 \times 0.63\ \mu$m^2. The atom number histogram has 5000 events taken from one of the six sites showing clear separation of the zero-atom background from the one-atom peak. The solid line is a Poissonian model fitted to the one-atom peak.

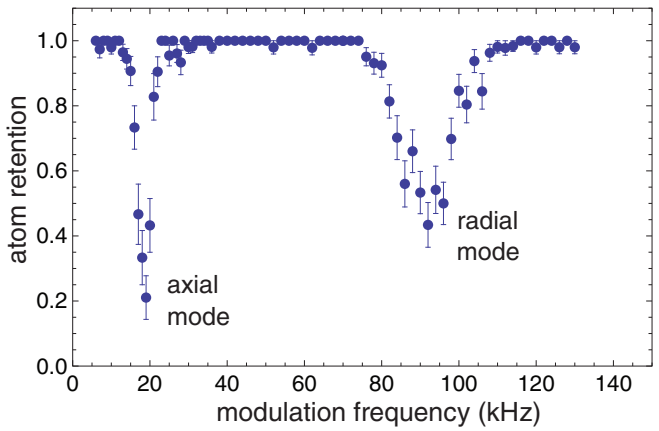

FIG. 9. (Color online) Parametric heating measurement of trap frequencies.

optical efficiency from the fiber end to the atoms including the array generation and subsequent relay and focusing optics is about 50%. With a power of 1.5 W at the atoms divided into 16 beams we achieve trap depths of $\sim 830\ \mu$K in an array with $d = 3.8\ \mu$m and $s = 2.1$. The array period is longer than is common in many optical lattice experiments and is chosen to be compatible with magic trapping of high-n Rydberg states [6]. The close-to-4-μm trap spacing also facilitates addressing single sites using laser beams focused to few-micron waists [14].

Figure 8 shows fluorescence images of the trapped atoms and a histogram of single-atom events. In the histogram the single-atom signal is clearly seen, with the loading rate varying from 50% to 60% between sites. The average loading rate is 52.5%, which is sub-Poissonian, and also slightly above that expected from light-assisted two-body loss, or collisional blockade [27]. We do not observe any events with two or more atoms in the trap, although we cannot exclude the possibility that we load two atoms but lose them rapidly during the fluorescence imaging exposure.

To compare the trap depth with theoretical calculations we measured the trap oscillation frequencies. Equations (5) give the frequencies as $\omega_x = 2\pi \times 39$ kHz and $\omega_z = 2\pi \times 6.4$ kHz. To measure the trap oscillations the intensity of the trapping light was modulated at frequency f. When the frequency matches $2\omega_0/2\pi$ the atoms will be heated and leave the trap. After we confirmed the initial presence of an atom in the trap site the modulation was applied for 100 ms for $f < 35$ kHz and for 5 ms for $f > 35$ kHz. Then we took a second image to measure the retention of the atom in the trap. For each modulation frequency the measurement was repeated 200 times. The observed spectrum for one of the traps is presented in Fig. 9.

Two resonances can be easily identified: one around 18 kHz, corresponding to $\omega_z/2\pi = 9$ kHz (axial frequency) and a broader resonance centered at 90 kHz ($\omega_x/2\pi = 45$ kHz). The radial frequency agrees to about 10% with that calculated based on our known trap geometry and optical power. The axial frequency is about 50% higher than expected. We have observed that individual focused beams in the array do not have an ideal Gaussian profile and diverge more rapidly than for a Gaussian with the same waist parameter; i.e., the beam quality factor is $M^2 > 1$. This fast divergence has a minimal effect on the radial trap frequencies but will increase the axial frequencies, which is consistent with our observations.

For future experiments with qubits we wish the traps to be well aligned on a regular grid. Fits to the image in Fig. 8 reveal an average spacing of $d = 3.90\ \mu$m, close to the expected 3.8 μm. We find a maximum deviation of the atomic centroids from a regular grid of $\sim$0.6 μm. This deviation is very sensitive to optical alignment and we attribute this to the residual influence of interference between diagonally separated beams in each unit cell. The lifetime of atoms in the traps is measured with all light switched off except for the 780-nm trapping light. Measured $1/e$ lifetimes range from 3.7 to 11 s for the different sites. The lifetime limit due to collisions with untrapped background gas was measured to be $\sim$20 s using a several-millikelvin-deep, red-detuned, single-beam trap formed with 1040-nm light. We attribute the shorter lifetimes in the GBA to the lower trap depth and, possibly, imperfections in the trap potentials. As with the deviations in the atomic centroids we find the lifetimes to be very sensitive to adjustment of the alignment in the array-forming optics. Due to the sensitivity to optical alignment we have studied the performance of the full-incoherent array as described in the following.

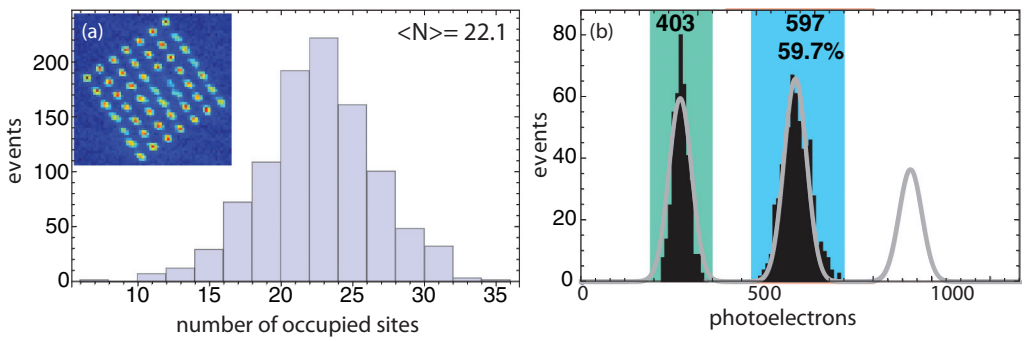

FIG. 10. (Color online) Atom trapping in a 49-site full-incoherent array. (a) Distribution of number of occupied sites with fluorescence image. The fluorescence image is an average over 100 atom loading shots, with noise filtered by performing a principal-component analysis on the data set and combining the 49 components with the highest eigenvalues to form the image. (b) Histogram from one of the sites, showing a 59.7% single-atom loading rate. The solid line is a Poissonian model fitted to the one-atom peak.

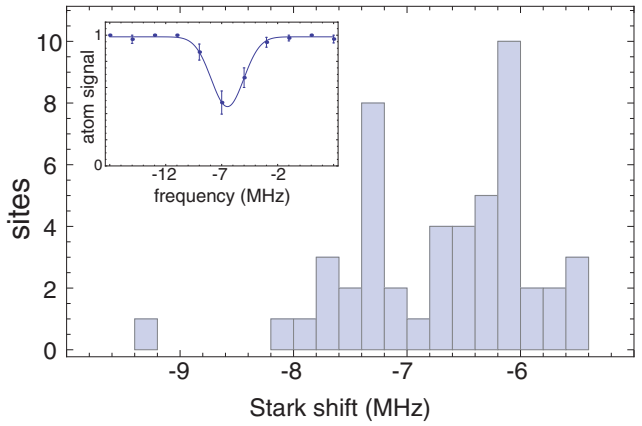

FIG. 11. (Color online) Stark shift of the $6s_{1/2}$, $f = 4 \leftrightarrow 6p_{3/2}$, $f = 5$ transition in the 49-site array. Inset: Atom blow-away curve as the laser frequency is scanned.

B. Full-incoherent array

Atom trapping in the 49-site full-incoherent array is shown in Fig. 10. For these experiments we used two separate 780-nm laser systems: the frequency-doubled 1560-nm source used for the half-incoherent array experiments and a single-frequency Ti:Sa laser, also operating near 780 nm. The two laser systems were adjusted to have wavelengths within 1 nm of each other. The optical efficiency for the setup in Fig. 7 from the fiber ends to the atoms including the array generation and subsequent relay and focusing optics is about 60%. The trap depth is given by Eq. (9). With a power of 2.5 W out of each fiber we projected a total of 3 W onto the atoms, giving 47 mW in each of the 64 beams. This resulted in a trapping potential of $\sim$570 μK in an array with $d = 3.8$ μm and $s = 2.1$. Atom trapping was observed with a potential as low as $\sim$340 μK. The data presented below were all taken with $\sim$570-μK-deep traps. Figure 10 shows a fluorescence image of the array with a single-atom loading histogram. The average atom lifetime in the array was about 1.5 s. Single-atom exposure parameters were the same as for the half-incoherent array.

We see that the average number of occupied sites in each loading event is approximately $22/49 = 45\%$ of the array size. Single atoms are loaded into all sites, although about five sites have substantially lower loading rates than the average and about five sites have loading rates above 60%. We believe the loading rate could be further improved at all sites using the technique of repulsive light-assisted collisions [28]. The regularity of the atomic positions is significantly better in this array than in the half-incoherent method. Fitting the fluorescence image to a regular grid we find that the average deviation of the atomic centroids from a regular grid is about 0.35 μm, which is close to half the deviation seen in the half-incoherent array.

An important consideration for qubit experiments is that trap-induced Stark shifts on atomic transitions used for state control are uniform across the array. The trapping sites in the GBA are not perfectly dark; there is a nonzero intensity I_c at the center of each trap. This is intentional and is beneficial for correct magic trapping of ground-Rydberg state transitions [6]. We have verified the uniformity of the intensity I_c at each site by scanning across the $6s_{1/2}$, $f = 4 \leftrightarrow 6p_{3/2}$, $f = 5$ transition with a 5-μs pulse from a single unbalanced beam to blow away the atoms. The data in Fig. 11 show a mean transition Stark shift relative to the value for an atom outside the lattice of -6.7 MHz, with a standard deviation of 0.8 MHz. The typical fractional deviation of the Stark shift is thus $0.8/6.7 = 12\%$. From Eqs. (8) and (9) the intensity at trap center is related to the effective trapping intensity by $I_c/I_t = 2e^{-s^2/2}(1 - 2e^{-s^2/2})$, giving $I_c/I_t = 0.17$ at $s = 2.1$. The average light shift of the ground state at trap center is thus 0.17×570 μK $= 97$ μK, with a standard deviation of about 10 μK.

The site-to-site shifts may come into play when we consider dephasing of qubits encoded in the $f = 3,4$ hyperfine clock states, which have a transition frequency of 0.0092 THz. At our detuning of 72 nm (32.5 THz) from the Cs D2 transition the standard deviation of the clock frequency across the array due to trap-induced Stark shifts is approximately 10 μK $\times$ $\frac{0.0092}{0.0092+32.5} = 0.0028$ μK or $\sim$60 Hz. If left uncompensated, this would cause dephasing of qubits in different sites on a time scale of a few milliseconds. With good laser stabilization these shifts will be static and it is possible to keep track of them. Alternatively, much longer coherence times should be possible using additional plane-wave optical fields to compensate the differential Stark shift [29].

V. CONCLUSIONS

In summary, we have designed and demonstrated a two-dimensional optical trap array using weakly overlapping Gaussian beams. Single Cs atoms are loaded into the array with an approximately 45% average filling factor. High-fidelity detection of single atoms is achieved using fluorescence imaging. The moderately large spacing and blue-detuned character of the array make it well suited for demonstrating quantum gates with Rydberg-state-mediated interactions. Results of quantum gate experiments in the array using microwave and optical fields for state control will be reported elsewhere.

ACKNOWLEDGMENTS

This work was supported by the IARPA MQCO program through ARO Contract No. W911NF-10-1-0347 and by DARPA.

[1] D. Meschede and A. Rauschenbeutel, Adv. At. Mol. Opt. Phys. **53**, 75 (2006).
[2] M. Saffman, T. G. Walker, and K. Mølmer, Rev. Mod. Phys. **82**, 2313 (2010).
[3] A. Negretti, P. Treutlein, and T. Calarco, Quant. Info. Proc. **10**, 721 (2011).
[4] M. Schlosser, S. Tichelmann, J. Kruse, and G. Birkl, Quant. Info. Proc. **10**, 907 (2011).

[5] R. A. Cline, J. D. Miller, M. R. Matthews, and D. J. Heinzen, Opt. Lett. **19**, 207 (1994).
[6] S. Zhang, F. Robicheaux, and M. Saffman, Phys. Rev. A **84**, 043408 (2011).
[7] T. Wilk, A. Gaëtan, C. Evellin, J. Wolters, Y. Miroshnychenko, P. Grangier, and A. Browaeys, Phys. Rev. Lett. **104**, 010502 (2010).
[8] L. Isenhower, E. Urban, X. L. Zhang, A. T. Gill, T. Henage, T. A. Johnson, T. G. Walker, and M. Saffman, Phys. Rev. Lett. **104**, 010503 (2010).
[9] X. L. Zhang, L. Isenhower, A. T. Gill, T. G. Walker, and M. Saffman, Phys. Rev. A **82**, 030306(R) (2010).
[10] T. Keating, K. Goyal, Y.-Y. Jau, G. W. Biedermann, A. J. Landahl, and I. H. Deutsch, Phys. Rev. A **87**, 052314 (2013).
[11] A. Carr and M. Saffman, Phys. Rev. Lett. **111**, 033607 (2013).
[12] R. Dumke, M. Volk, T. Müther, F. B. J. Buchkremer, G. Birkl, and W. Ertmer, Phys. Rev. Lett. **89**, 097903 (2002).
[13] S. Bergamini, B. Darquié, M. Jones, L. Jacubowiez, A. Browaeys, and P. Grangier, J. Opt. Soc. Am. B **21**, 1889 (2004).
[14] C. Knoernschild, X. L. Zhang, L. Isenhower, A. T. Gill, F. P. Lu, M. Saffman, and J. Kim, Appl. Phys. Lett. **97**, 134101 (2010).
[15] K. Gillen-Christandl and G. D. Gillen, Phys. Rev. A **82**, 063420 (2010).
[16] K. D. Nelson, X. Li, and D. S. Weiss, Nat. Phys. **3**, 556 (2007).
[17] W. S. Bakr, J. I. Gillen, A. Peng, S. Fölling, and M. Greiner, Nature (London) **462**, 74 (2009).
[18] J. F. Sherson, C. Weitenberg, M. Endres, M. Cheneau, I. Bloch, and S. Kuhr, Nature (London) **467**, 68 (2010).
[19] C. Weitenberg, M. Endres, J. F. Sherson, M. Cheneau, P. Schauß, T. Fukuhara, I. Bloch, and S. Kuhr, Nature (London) **471**, 319 (2011).
[20] K. I. Petsas, A. B. Coates, and G. Grynberg, Phys. Rev. A **50**, 5173 (1994).
[21] M. Weidemüller, A. Görlitz, T. W. Hänsch, and A. Hemmerich, Phys. Rev. A **58**, 4647 (1998).
[22] L. Isenhower, W. Williams, A. Dally, and M. Saffman, Opt. Lett. **34**, 1159 (2009).
[23] P. Xu, X. He, J. Wang, and M. Zhan, Opt. Lett. **35**, 2164 (2010).
[24] G. Li, S. Zhang, L. Isenhower, K. Maller, and M. Saffman, Opt. Lett. **37**, 851 (2012).
[25] V. V. Ivanov, J. A. Isaacs, M. Saffman, S. Kemme, A. Ellis, G. Brady, J. Wendt, G. W. Biedermann, and S. Samora, arXiv:1305.5309.
[26] H. Dammann and K. Görtler, Opt. Commun. **3**, 312 (1971).
[27] N. Schlosser, G. Reymond, and P. Grangier, Phys. Rev. Lett. **89**, 023005 (2002).
[28] T. Grünzweig, A. Hilliard, M. McGovern, and M. F. Andersen, Nat. Phys. **6**, 951 (2010).
[29] A. G. Radnaev, Y. O. Dudin, R. Zhao, H. H. Jen, S. D. Jenkins, A. Kuzmich, and T. A. B. Kennedy, Nat. Phys. **6**, 894 (2010).